International Journal of Multiphase Flow 35 (2009) 270–276

Contents lists available at ScienceDirect

International Journal of Multiphase Flow

journal homepage: www.elsevier.com/locate/ijmulflow

# An improved constitutive model for concentrated suspensions accounting for shear-induced particle migration rate dependence on particle radius

Marc S. Ingber [a], Alan L. Graham [b,*], Lisa A. Mondy [c], Zhiwu Fang [d]

[a] Department of Mechanical Engineering, University of New Mexico, Albuquerque, NM 87131, USA
[b] Los Alamos National Laboratory, Los Alamos, NM 87545, USA
[c] Sandia National Laboratories, Albuquerque, NM 87185, USA
[d] Department of Systems Informatics, Amgen Inc., One Amgen Center Dr., Thousand Oaks, CA 91320, USA

ARTICLE INFO

*Article history:*
Received 19 May 2008
Received in revised form 1 November 2008
Accepted 11 November 2008
Available online 21 November 2008

ABSTRACT

Several rheological constitutive equations for the modeling of dense suspensions in nonlinear shear flows have been developed over the last three decades. Although these models have been able to predict the correct steady-state solid-phase concentration profile, none have been able to follow the transient experimentally measured concentration profile over a range of suspended particle radii with a consistent set of diffusion coefficients. In this research, two improvements are made to the diffusive-flux model, namely, modeling the diffusion coefficients as linear functions of the so-called nonlinearity parameter and adding slip boundary conditions at the wall. A particle-level explanation for the linear dependence of the diffusion coefficients on the nonlinearity parameter is provided. With these two improvements, it is shown that the modified diffusive flux model can accurately predict the transient solid-phase concentration profile in a Couette device over a wide range of particle radii.

Published by Elsevier Ltd.

## 1. Introduction

Particle migration in suspension flows is important in a variety of scientific and engineering applications such as the transport of sediments, chromatography, composite materials processing, secondary oil recovery techniques, and sequestration processes in porous media to name a few. In particular, initially well mixed neutrally-buoyant particles in concentrated nonlinear suspension flows have been shown to undergo migration from high shear rate regions to low shear rate regions. For example, in a Couette device with rotating inner cylinder and stationary outer cylinder, the particles migrate towards the outer cylinder (Abbott et al., 1991, 1994, 2005), and in Poiseuille flows in conduits, the particles migrate towards the centerline of the conduits (Koh et al., 1993, 1997).

Several rheological models have been proposed to study suspension flows. Phillips et al. (1992) used the scaling arguments of Leighton and Acrivos (1987) to develop the so-called diffusive flux model. In this model, particle migration results from gradients in the shear rate, concentration and relative suspension viscosity. This model was refined by Fang et al. (2002) to account for the different rates of migration in the shear plane as opposed to the vorticity plane. In an alternative modeling approach based on the conservation laws of mass and momentum designated as the suspension balance model, the stress in the particle phase is described by a constitutive equation, and particle transport is driven by gradients in this stress (Jenkins and McTigue (1990, 1994, 1998)). The suspension balance model has been refined by Morris and Boulay (1999),Fang et al. (2002) and Shapley et al. (2004) to account for nonisotropic migration rates and to improve the modeling of particle velocity fluctuations. Additional rheological models based on mixture theory have been proposed by Buyevich (1995) and Pozarnik and Skerget (2003).

The models discussed above can satisfactorily describe the steady-state concentration profiles achieved in suspension flows; however, all of the models proposed to date show large discrepancies for transient concentration profiles with experimental data. In particular, these models predict that particle migration should scale with the radius of the particle squared. Unfortunately, the experimental data (Abbott et al., 1991, 1998, 2003) do not support this scaling, and hence, none of the models can be used to reliably predict transient concentration profiles. For example, experimental data for a wide-gap Couette device show that the migration rate should scale with the particle radius raised to anywhere from the 2.6 to 2.9 power.

In a recent study, Ingber et al. (2008) determined that a rough pair of interacting spheres in a nonlinear shear flow will migrate towards the low shear rate region of the flow field. Further, they found that the magnitude of the displacement of the center of gravity of the particle pair towards the low shear rate region scales linearly with the nonlinearity parameter, $\xi_{nl} = a|\nabla\dot{\gamma}|/(\dot{\gamma} + \dot{\gamma}_{NL})$ where $a$ is the particle radius, $\dot{\gamma}$ is the local shear rate, and $\dot{\gamma}_{NL}$ is the so-called nonlocal contribution to the shear rate as discussed in Section 3. This migration leads to a migration diffusivity which

* Corresponding author. Tel.: +1 505 655 3421.
*E-mail address:* graham@lanl.gov (A.L. Graham).

0301-9322/$ - see front matter Published by Elsevier Ltd.
doi:10.1016/j.ijmultiphaseflow.2008.11.003

also is a function of the $\xi_{nl}$. Based on these results, it can be conjectured that the diffusion coefficients in the diffusive flux model should also be linear functions of the $\xi_{nl}$.

In this research, two modifications are made to the diffusive flux model. First, the diffusion coefficients are modeled as linear functions of the nonlinearity parameter. However, this modification in itself leads to essentially cubic scaling of migration on the particle radius which is somewhat larger than found in experiment. To reduce the scaling to match experimental results in the wide-gap Couette, velocity slip boundary conditions are imposed at the wall. It is shown that, with these two modifications, it is possible to match experimental results with model predictions using a consistent set of model diffusion coefficients over a wide range of particle radii.

## 2. The diffusive-flux model

The multiphase systems considered are solid particles suspended in a Newtonian fluid. For neutrally-buoyant particles, the balance equations for an incompressible suspension are given by

$$\nabla \cdot \mathbf{u_s} = 0 \tag{1}$$

$$\frac{D\rho \mathbf{u_s}}{Dt} = \nabla \cdot \underset{\approx}{\boldsymbol{\sigma}} \tag{2}$$

where

$$\frac{D}{Dt} = \frac{\partial}{\partial t} + \mathbf{u_s} \cdot \nabla \tag{3}$$

is the substantial derivative and $\mathbf{u_s}$ is the suspension velocity. The suspension stress tensor $\underset{\approx}{\boldsymbol{\sigma}}$ is given by

$$\underset{\approx}{\boldsymbol{\sigma}} = -p\,\underset{\approx}{\delta} + 2\eta(\phi)\,\underset{\approx}{D} \tag{4}$$

where $p$ is the suspension pressure, $\phi$ is the volume fraction of solids in the suspension, $\eta(\phi)$ is the effective suspension viscosity, $\underset{\approx}{D}$ is the suspension deformation rate tensor, and $\underset{\approx}{\delta}$ is the Kronecker-$\delta$ function.

The effective suspension viscosity is modeled using the Krieger correlation. That is, $\eta = \eta_r \eta_s$ where $\eta_s$ is the solvent viscosity and $\eta_r$ is the relative viscosity given by

$$\eta_r = \left(1 - \frac{\phi}{\phi_m}\right)^{-\alpha} \tag{5}$$

where $\phi_m$ is the maximum solid volume fraction for which the suspension exhibits fluid behavior. The value of $\phi_m$ depends on several factors as discussed by Subia et al. (1998). In this research, $\phi_m$ is chosen to be 0.68 and $\alpha$ is chosen to be 1.82.

The concentration evolution equation is given by

$$\frac{D\phi}{Dt} = -\nabla \cdot \mathbf{N} \tag{6}$$

in which $\mathbf{N}$ has two contributions, one due to interparticle hydrodynamic interactions, $\mathbf{N_c}$, and one due to spatial variations in viscosity, $\mathbf{N}_\eta$.

To account for the nonisotropic behavior of the particle flux at a point, two fluxes are reformulated based on a flow-aligned tensor, $Q$, written in terms of shear-axis coordinates $\delta_1$, $\delta_2$, and $\delta_3$ (Fang et al., 2002). The shear axes are based on the shear surfaces moving with the ambient flow. At any time, $\delta_1$ and $\delta_3$ are tangent to the shearing surface. In particular, $\delta_1$ is in the direction of the streamline and $\delta_3$ is in the direction of the velocity gradient. In this coordinate system, the flow-aligned tensor $\mathbf{Q}$ is given by

$$\mathbf{Q} = \begin{pmatrix} \lambda_1 & 0 & 0 \\ 0 & \lambda_2 & 0 \\ 0 & 0 & \lambda_3 \end{pmatrix} \tag{7}$$

The two particle flux terms are then modeled as

$$\mathbf{N_c} = -K_c a^2 \phi \nabla \cdot (\dot{\gamma}\phi \mathbf{Q}) \tag{8}$$

and

$$\mathbf{N}_\eta = -K_\eta a^2 \phi (\dot{\gamma}\phi \mathbf{Q}) \cdot \nabla \ln \eta \tag{9}$$

In order to achieve the correct concentration profiles in a parallel plate and cone and plate geometry, it was determined that $\lambda_1 = \lambda_2 = 2\lambda_3$ (Fang et al., 2002).

However, in the circular Couette flow geometry, the diffusive flux equation reduces to its original form given by Phillips et al. (1992). That is

$$\frac{\partial \phi}{\partial t} = \frac{a^2}{r}\frac{\partial}{\partial r}\left\{ r\left[ K_c\left(\phi^2 \frac{\partial \dot{\gamma}}{\partial r} + \phi\dot{\gamma}\frac{\partial \phi}{\partial r}\right) + K_\eta(\dot{\gamma}\phi^2)\frac{1}{\eta}\frac{d\eta}{d\phi}\frac{\partial \phi}{\partial r}\right]\right\} \tag{10}$$

## 3. Motivation for modifications to the diffusive flux model

As seen in Eqs. (6), (8) and (9) or Eq. (10), the migration rate of the classical diffusive flux model scales quadratically with the particle radius, $a$. One of the modifications implemented in this research is to make the diffusion coefficients, $K_c$ and $K_\eta$, linear functions of the nonlinearity parameter, $\xi_{nl}$, given by

$$\xi_{nl} = \frac{a|\nabla \dot{\gamma}|}{\dot{\gamma} + \dot{\gamma}_{NL}} \tag{11}$$

where $\dot{\gamma}_{NL}$ is the so-called nonlocal contribution to the shear rate. As discussed by Miller et al. (2006), a small constant nonlocal contribution is added to the local shear rate to take into account the fact that the RMS of $\dot{\gamma}$ is larger than the mean shear rate resulting from the finite size of the spheres. In this research, the nonlocal shear rate is modeled as

$$\dot{\gamma}_{NL} = \frac{a}{R_o}\dot{\gamma}_o \tag{12}$$

where $R_o$ is the outer radius of the Couette and $\dot{\gamma}_o$ is the shear rate at the outer edge of the Couette. The nonlocal shear rate plays a small role in the Couette flow considered here, but can have a large influence for other flow fields such as Poiseuille flows.

The motivation for this modification comes from considering two-sphere interactions in a Couette flow field. In previous research, Ingber et al. (2008) determined, using a traction-corrected boundary element method (TC-BEM), that there is a net displacement of the center of gravity of a pair of rough spheres interacting in a quadratic flow towards the low shear rate region of the flow field. Further, they determined that the magnitude of this net displacement scaled linearly with the nonlinearity parameter. In a sense, $\xi_{nl}$ describes the degree of nonlinearity of the flow field experienced by the spheres at various locations within the flow. The TC-BEM simulations are repeated here for circular Couette flow. In particular, the far field circumferential velocity profile is given by

$$u_\theta = cr/2 + d/r \tag{13}$$

where $u_\theta$ is the circumferential velocity, $c = -2/3$ and $d = 1323$, which corresponds to a Couette device of inner diameter of 31.50 and outer diameter of 62.99. Note that no physical walls are included in the simulations. The two spheres of radius 1 are initially placed at the locations $r_1^i, \theta_1^i$ and $r_2^i, \theta_2^i$ where $r$ is the radial distance measured from the center of the Couette and $\theta$ is the polar angle measured from the positive $x$-axis as shown in Table 1. The spheres have a roughness, $\delta$, given by $\delta/a = 0.01$. The roughness model is implemented by restricting the relative normal motion of the two spheres when they reach a separation of $\delta$ (Ingber et al., 2008). The initial angle that the lines generated from the center of the Couette to the centers of the two spheres make with each other is 45°.

**Table 1**
Simulation results for two rough spheres in circular Couette flow.

| $r_1^i,\theta_1^i$ | $r_2^i,\theta_2^i$ | $r_{ave}^i$ | *NLP* | $r_1^f,\theta_1^f$ | $r_2^f,\theta_2^f$ | $r_{ave}^f$ |
|---|---|---|---|---|---|---|
| 30.200,−0.7854 | 30.500,0.000 | 30.35 | 0.0659 | 29.829,−1.716 | 30.905,−2.512 | 30.367 |
| 32.700,−0.7854 | 33.000,0.000 | 32.85 | 0.0609 | 32.330,−0.840 | 33.402,−1.623 | 32.866 |
| 35.200,−0.7854 | 35.500,0.000 | 35.350 | 0.0566 | 34.827, −0.500 | 35.901,−1.281 | 35.364 |
| 37.700,−0.7854 | 38.000,0.000 | 37.850 | 0.0528 | 37.342,−0.729 | 38.384,−1.515 | 37.863 |

The inner cylinder of the Couette is rotated causing the inner sphere to interact with and overtake the outer sphere. The simulation is continued until the angle that the lines generate from the center of the Couette to the centers of the two spheres is once again 45° whence the simulation is stopped. Also shown in Table 1 are the initial average radial position of the two spheres $r_{ave}^i$, the corresponding value of the nonlinearity parameter, $\xi_{nl}$, at that radial position, the final positions of two spheres $r_1^f,\theta_1^f$ and $r_2^f,\theta_2^f$, and the final average radial position of the two spheres $r_{ave}^f$. The difference between the final average radial position of the two spheres and the initial average radial position of the two spheres represents the net permanent displacement of the center of gravity of the particle pair, $\Delta r_{cg}$. This net permanent displacement as a function of the $\xi_{nl}$ is shown in Fig. 1. As seen in the figure similar to the result for quadratic flow (Ingber et al., 2008), the net permanent displacement of the particle pair scales essentially linearly with the nonlinearity parameter.

Although the above simulations were performed for an isolated rough particle pair in Couette flow, they do provide evidence that the net migration induced by particle interactions in dense suspensions should also be functions of the nonlinearity parameter. Further, based on the linear relationship shown in Fig. 1, it is not unreasonable to presume a linear relationship between the diffusion coefficients in the diffusive flux model and the nonlinearity parameter.

## 4. Modifications to the diffusive flux model

Two modifications to the diffusive flux model are implemented in this research. As discussed above, the first modification is to make the diffusion coefficient, $K_c$, a linear function of the nonlinearity parameter, $\xi_{nl}$. That is, $K_c$ is modeled as

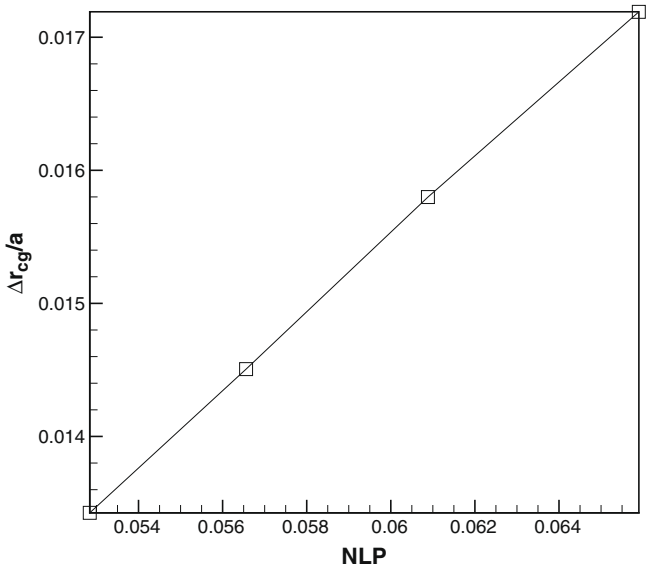


**Fig. 1.** The net parameter displacement of a particle pair $\Delta r_{cg}$ as a function of the nonlinearity parameter, $\xi_{nl}$ for a roughness $\delta/a = 0.01$.

$$K_c = \kappa\xi_{nl} = \kappa\frac{a|\nabla\dot{\gamma}|}{\dot{\gamma} + \dot{\gamma}_{NL}} \tag{14}$$

where $\kappa$ is a modeling parameter to be determined by comparing model predictions with experimental data. The ratio of the diffusion coefficients $K_c/K_\eta$ is given by the ensemble local model proposed by Tetlow et al. (1998). That is,

$$K_c/K_\eta = r_k\phi \tag{15}$$

where the proportionality constant $r_k$ is chosen to best match steady-state results for the Couette device for a given bulk concentration, $\bar{\phi}$. Hence, $K_\eta$ is also a linear function of the nonlinearity parameter.

The second modification to the diffusive flux model is the adoption of a slip velocity boundary condition. The velocity field $\mathbf{u_s}$ is the volume-averaged suspension velocity over the fluid and solid phases. Because the particles cannot physically occupy the space adjacent to a wall as effectively as in the bulk of the fluid, an "apparent slip layer" which is essentially devoid of particles forms next to the wall (Kalyon, 2005). This slip layer has a greatly reduced effective viscosity compared to the bulk suspension and results in an "apparent slip velocity" at the wall (Soltani and Yilmazer, 1998). This slip velocity has been measured experimentally by Jana et al. (1995), Soltani and Yilmazer (1998), Gulmus and Yilmazer (2005) and Mondy et al. (2005). In general, these researchers found that the effective slip increased with particle size and concentration. The slip boundary condition is given by

$$\beta a\mathbf{T}\cdot\mathbf{n} = \eta_s(\mathbf{u_p} - \mathbf{u_f})\cdot\mathbf{t} \tag{16}$$

where $\mathbf{T}$ is the traction on the solid boundary wall, $\mathbf{n}$ and $\mathbf{t}$ are the normal and tangential unit vectors to the wall, respectively, $\mathbf{u_p}$ and $\mathbf{u_f}$ are the particle phase and fluid phase velocities, respectively, and $\beta$ is the non-dimensional slip coefficient. In general, $\beta$ is a function which increases monotonically with particle diameter and solid-phase concentration. When $\beta = 0$, there is no slip on the wall, and when $\beta = \infty$, there is perfect slip.

The suspension phase velocity is given by

$$\mathbf{u_s} = (1-\phi)\mathbf{u_f} + \phi\mathbf{u_p} \tag{17}$$

Substituting Eq. (17) into Eq. (16) and noting that all velocities must be tangent to the wall yields

$$u_s^t = u_f^t + \frac{a\phi\beta}{\eta_s}\mathbf{T}\cdot\mathbf{n} = u_b^t + a\phi\eta_r\beta\dot{\gamma} \tag{18}$$

where $u_s^t$ is the tangential component of $\mathbf{u_s}$, $u_f^t$ is the tangential component of $\mathbf{u_f}$, $u_b^t$ is the tangential component of the boundary which is the same as $u_f^t$ because of the no-slip fluid boundary condition.

For future reference to the results of Jana et al. (1995), it should be noted that they defined their slip coefficient, $\beta_o$, as

$$u_s^t = u_b^t + a\beta_o\dot{\gamma} \tag{19}$$

Hence,

$$\beta_o = \phi\eta_r\beta \tag{20}$$

The diffusive flux equation, Eq. (10), subject to the slip boundary condition, Eq. (18), is solved using a standard foward-time, central-space (FTCS) finite difference method. Since the method is

explicit, the nonlinearity parameter, $\xi_{nl}$, which is a function of the local shear rate and shear rate gradient, can be evaluated from the previous time step. Appropriate convergence tests have been performed to assure the quality of the numerical results.

## 5. Model tuning and results

The tuning of the modified diffusive flux model is performed by comparing model predictions to a series of experiments performed in a wide-gap Couette device. Details of the experiments are described by Tetlow (1997) and Hsiao et al. (2005). To nondimensionalize the governing equations, the outer radius of the Couette apparatus, $R_o$, is taken as the length scale, $\omega R_o$ is taken as the velocity scale, where $\omega$ is the inner cylinder angular rotation rate, and $1/\omega$ is taken as the time scale. To match experimental results, the inner cylinder radius $R_i$ is given by $R_i/R_o = 0.25$.

There are several adjustable (tuning) parameters in the diffusive flux model. The model is tuned here to best match the experimental results at a bulk concentration of $\bar{\phi} = 50\%$. The parameters $\phi_m$ and $\alpha$ used in the Krieger (1972) model for the suspension viscosity are chosen based on rheometric viscosity data as discussed in Section 3. The $r_k$ in Eq. (15) for the ratio of the diffusion coefficients $K_c/K_\eta$ is taken as a function of the bulk concentration $\bar{\phi}$ and is chosen so that diffusive flux model best matches steady state experimental data. For the case $\bar{\phi} = 50\%$, $r_k = 1.5$ (Tetlow et al. (1998)).

The determination of $\kappa$ in Eq. (14) and the slip coefficient $\beta$ in Eq. (16) is more involved. The determination of $\kappa$ is performed first. However, this is problematic in the sense that without the knowledge of $\beta$, it is impossible to determine $\kappa$ since increasing slip at the wall decreases the rate of particle migration. Fortunately, the slip coefficient $\beta$ has been determined experimentally for very similar conditions by Jana et al. (1995). The determination of $\beta$ will be deferred to later.

To determine the parameter $\kappa$, simulations are performed for sphere size given by $a/R_o = 2.10 \times 10^{-3}$ corresponding to 50 μm spheres at a bulk concentration of $\bar{\phi} = 50\%$ for which $\beta = 1/4$ (Jana et al., 1995). It is presumed that the rate of particle migration scales as $(a/a_{ref})^n$ where $a_{ref}$ is an arbitrary reference sphere radius as discussed by Tetlow et al. (1998) and Hsiao et al. (2003). In order to determine the optimum $\kappa$, it is necessary to simultaneously determine the optimum scaling exponent $n$. First, optimization is performed to determine the best $\kappa$ for a presumed value of $n$, and second, optimization is performed to determine the best scaling exponent $n$ with its associated $\kappa$.

The optimization is performed using the so-called difference measure, $DM$, defined by

$$DM = \frac{2}{R_o^2 - R_i^2} \int_{R_i}^{R_o} |\phi(r) - \bar{\phi}| r dr \tag{21}$$

where $\phi$ is the circumferentially averaged solid-phase concentration and $\bar{\phi}$ is the bulk concentration of the suspension. That is, the difference measure $DM$ represents the degree to which the transient concentration profile within the Couette apparatus has departed from the initial uniform concentration profile. The difference measure is taken to be a function of the effective strain, $S_e$, defined by

$$S_e = N_i \left( \frac{a}{a_{50}} \right)^n \tag{22}$$

where $N_i$ is the number of revolutions of the inner cylinder and $a_{50}$ is the arbitrary reference radius of 50 microns.

The optimum value for $\kappa$ at a presumed value of the scaling exponent $n$ can be determined by computing the least-squares error between the modified diffusive flux model and 23 discrete experimental data points for the difference measure generated with 64, 328, 800, and 1588 μm particles. A plot of this least-squares error as a function of $\kappa$ for $n = 2.8$ is shown in Fig. 2. Once the minimum least-squares error is determined for each $n$, this local minimum can be plotted as a function of $n$ as shown in Fig. 3. It is seen in the figure that the minimum least-squares error occurs at a value of the scaling exponent given by $n = 2.8$.

It is interesting to note that Tetlow et al. (1998) determined an optimum scaling exponent of $n = 2.9$ based on the same experimental data. However, Tetlow et al. performed their optimization based on a statistical predictive model which was an exponential curve fit to the experimental data. In particular, their predictive model never approached a steady state, and hence, data at large values of effective strain were not approximated particularly well. Based on this analysis, the global optimal value of $\kappa$ can be determined from Fig. 2 and is given by $\kappa = 4.7$.

The actual comparison between the experimental data and the numerical prediction of the modified diffusive flux model with optimized $\kappa$ and $n$ is shown in Fig. 4. As seen in the figure, the numerical predictions model the data quite well over a range of particle radii spanning from 50 to 1588 μm.

The numerical curve in Fig. 4 was generated for one size sphere only characterized by $a/R_o = 2.10 \times 10^{-3}$ corresponding to a 50 micron radius. It has yet to be shown that the modified diffusive flux can be used over a range of sphere radii. If no slip boundary conditions are imposed, it can be shown that the modified diffusive flux model would predict a particle migration scaling with the cube of the sphere radius, i.e., $n = 3$ which contradicts the experimental data as discussed above.

For suspensions containing spheres of larger radii, the slip parameter $\beta$ is adjusted using the bisection method so that the difference measure reaches a value of 0.07 at the same effective strain as was the case for the 50 μm spheres. Choosing the value of the difference measure of 0.07 is somewhat arbitrary but did collapse the curves for the various radii considered quite nicely as seen in Fig. 5. The model correctly predicts the migration rate for particles of essentially any radius, if one adjusts the slip parameter, $\beta$, is adjusted appropriately. The values of $\beta$ used to get the agreement shown in Fig. 5 is shown in Fig. 6. Although there are no known measurements for the slip coefficient for the larger-sized spheres, the results are at least qualitatively reasonable as the slip will increase with sphere diameter. A comparison between the modified

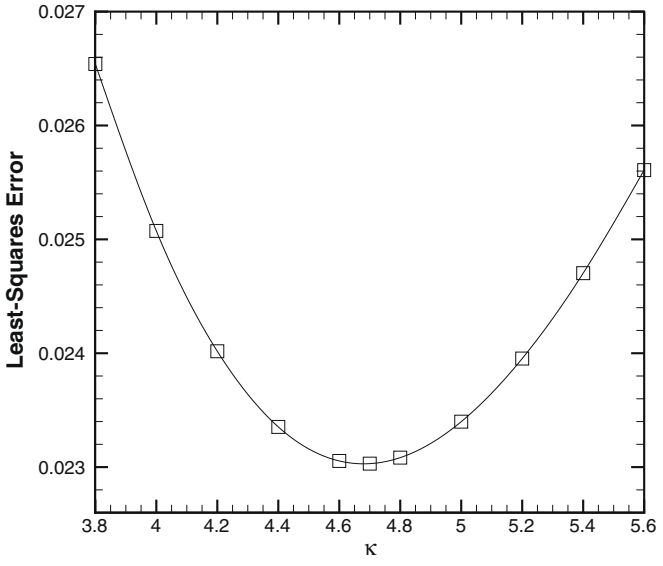


**Fig. 2.** The least-squares error between the modified diffusive flux model and experimental data for the difference measure as a function of the model parameter $\kappa$ at a value of the scaling exponent $n = 2.8$.

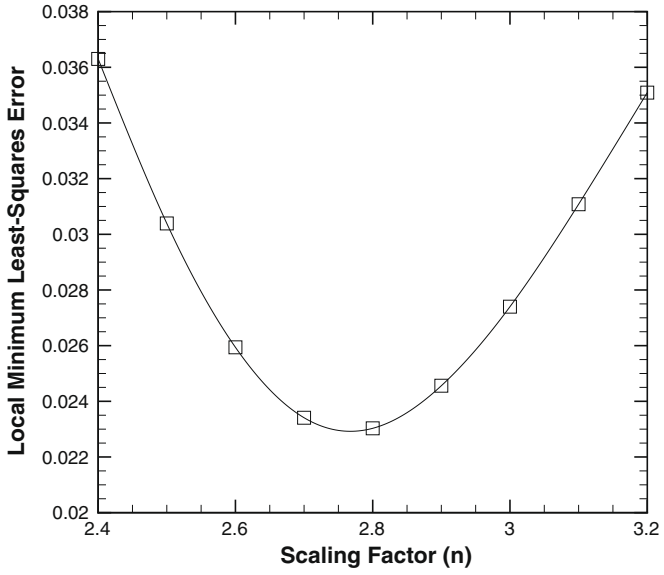


**Fig. 3.** The least-squares error between the modified diffusive flux model and experimental data as a function of the scaling exponent $n$.

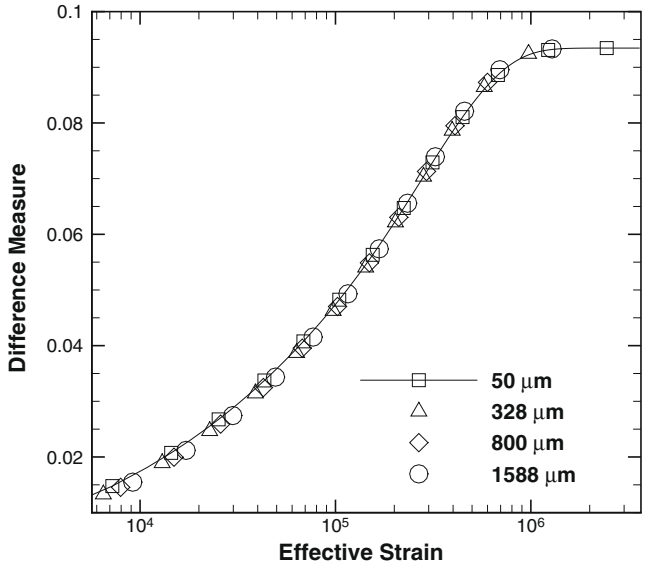


**Fig. 5.** The difference measure as a function of then effective strain with $n = 2.8$ as determined by the modified diffusive flux model for spheres of four different radii at a bulk concentration of $\bar{\phi} = 50\%$.

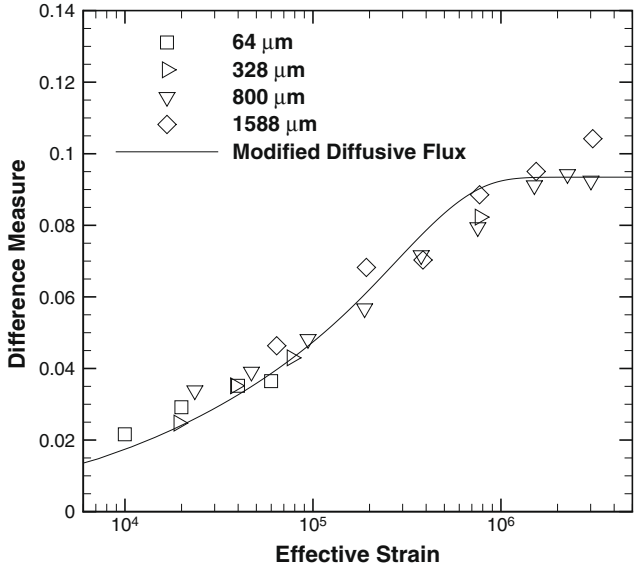


**Fig. 4.** A comparison of the difference measure determined by the modified diffusive flux model using a sphere radius of $a/R_o$=2.1008$e-3$ corresponding to a 50 micron radius and experimental measurements as a function of the effective strain with $n = 2.8$ for the bulk concentration of $\bar{\phi} = 50\%$.

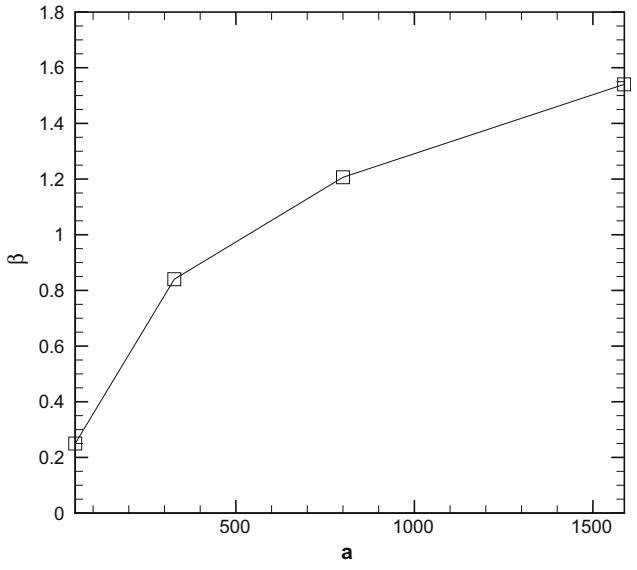


**Fig. 6.** The slip coeffcient $\beta$ as a function of sphere radius.

diffusive flux model predictions and experiment for the actual concentration profiles for the case of 64 μm spheres is shown in Fig. 7 at 200, 2000, and 8000 revolutions of the inner cylinder. Also shown in Fig. 7 is the steady-state concentration profile predicted by the modified diffusive flux model.

As discussed above, the modified diffusive flux model has been tuned to match experimental Couette data at a bulk solids concentration of 50%. Experimental data also exists for bulk solids concentrations of 35% and 42.5% (Hsiao et al., 2005). This tuned diffusive-flux model is compared to these two additional data sets in Figs. 8 and 9. Two changes are made to the modified diffusive flux model for the new data sets. First, the parameter $r_k$ from the ensemble local model of $K_c/K_\eta$ is taken from the optimized values to best replicate the steady state profile as determined by Tetlow et al. (1998). In particular, for $\bar{\phi} = 42.5\%$, $r_k = 1.35$, and for $\bar{\phi} = 35\%$, $r_k = 1.25$. Second, the scaling parameter $n$ is taken from the results of Hsiao et al. (2005). In particular, for $\phi = 42.5\%$, $n = 2.7$, and for $\bar{\phi} = 35\%$, $n = 2.6$. In both figures, the model result was determined using 50 μm spheres, and again, for the given scaling parameter $n$, model curves for spheres of different diameters could be essentially collapsed by adjusting the wall slip parameter. As seen in the figures, the model prediction for migration is somewhat slower than seen experimentally. This could be adjusted using the parameter $\kappa$. Nevertheless, the agreement between experiment and model predictions is relatively good.

## 6. Discussion

Rheological models for concentrated suspension flows have been investigated for the last 30 years. Although these models have

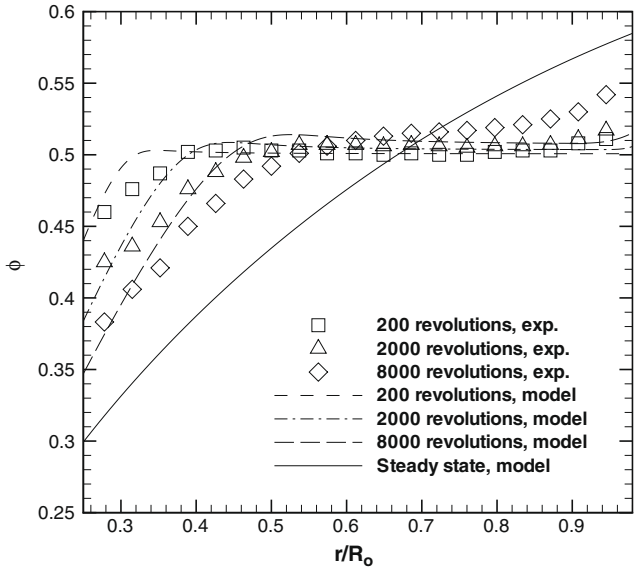


**Fig. 7.** A comparison of transient concentration profiles for 64 μm spheres at a bulk concentration of $\bar{\phi}$ = 50%.

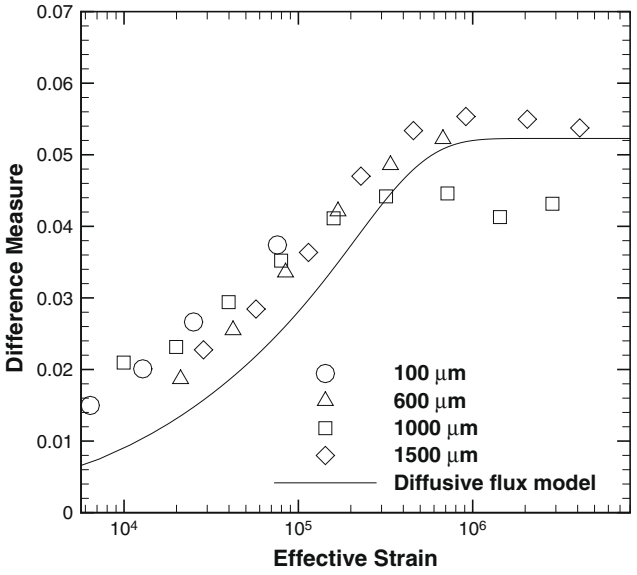


**Fig. 9.** The difference measure as a function of the effective strain with $n$ = 2.6 as determined by the modified diffusive flux model for spheres of four different radii at a bulk concentration of $\bar{\phi}$ = 35%.

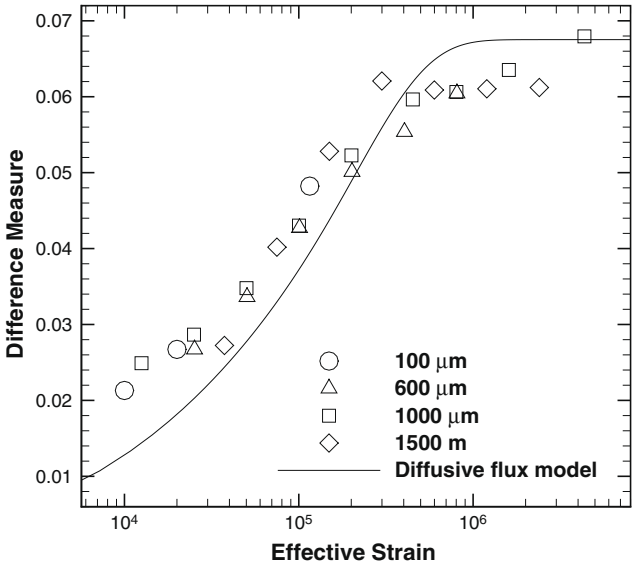


**Fig. 8.** The difference measure as a function of the effective strain with $n$ = 2.7 as determined by the modified diffusive flux model for spheres of four different radii at a bulk concentration of $\bar{\phi}$ = 42.5%.

been successful in predicting steady-state concentration profiles, they have been inadequate in predicting transient concentration profiles over a range of particle sizes. The central outstanding issue with these models for transient analysis is that the models all predict the migration rate to scale with the suspended particle radius squared. Unfortunately, this scaling simply has not been observed in wide-gap Couette experiments.

Two modifications to the diffusive flux model have been implemented to overcome the model's shortcomings. First, the diffusion coefficients have been made linear functions of the so-called nonlinearity parameter. This modification is motivated by considering the interaction of two spheres in circular Couette flow. Numerical simulations are performed using a traction-corrected boundary element method showing that the net displacement of the center of gravity of a rough pair of interacting spheres towards the low-shear-rate region of the flow field scales linearly with the nonlinearity parameter. These simulations imply that the net migration of a particle pair towards the low-shear-rate region of the flow field during a single interaction in a dense suspension should also depend on the local nonlinearity parameter. However, this modification by itself results in the migration rate of dense suspensions scaling with the particle radius cubed which is faster than observed experimentally. The second modification to the model is to introduce slip boundary conditions at the wall to enable the scaling of migration on particle radius to match experimental observation.

Model parameters of the modified diffusive flux model have been tuned so that the model predictions best match experiment. In particular, the original Krieger model for the relative viscosity and linear ensemble local model for the ratio of the two diffusion coefficients have been retained from previous research. In this research, a global search is performed to determine the optimal diffusion model parameter $\kappa$ and scaling exponent $n$ which is accomplished by performing a least squares error analysis between model predictions and experimental data at a bulk concentration of 50% in which the model predictions are performed using 50 μm spheres. This size suspended particle was chosen for the optimizations because it best matched the conditions under which Jana et al. (1995) measured the slip coefficient.

This approach for determining the scaling parameter $n$ is different than previous work in that the least squares average is taken between model predictions for difference measure and experiment as opposed to using a statistical predictive measure. The advantage of the current approach is that the model prediction attains a steady state whereas the predictive measure does not. The comparison between the tuned modified diffusive flux model using 50 μm spheres and experiment was quite good over the entire range of sphere radii used in the experiments. However, in order for the model predictions to scale with themselves at the optimal scaling parameter of $n$ = 2.8, the slip coefficient had to be appropriately adjusted. Although there are no known experimental measurements for the slip coefficient for larger size spheres, the results of this analysis are certainly reasonable as the slip coefficient increased with sphere radius which is consistent with previous research.

The modified diffusive flux model was also compared to data taken at bulk concentrations of 42.5 and 35%. Although the parameters for the ratio of the diffusion coefficients $r_k$ and scaling

parameter $n$ were taken from previous research, no effort was made to readjust the diffusion coefficient, $\kappa$. The comparisons between experiment and model predictions were fairly good despite this lack of tuning. It certainly would be possible to perform optimizations over the ensemble of experimental data rather than just the results at bulk concentration of 50%.

To assess the significance of the modifications to the diffusive flux model, consider the following comparison to the original diffusive flux model. The experimental data indicates, for a 50% bulk solid concentration, that the 1588 μm spheres reach a steady-state concentration profile in approximately 400 revolutions of the inner cylinder. This corresponds to an effective strain of approximately 3,200,000 based on the optimal scaling parameter of $n = 2.8$. However, using a scaling parameter of $n = 2.0$ as implicit in the original diffusive flux model, the original diffusive flux model would predict that on the order of 5200 revolutions would be required for the suspension containing 1588 μm spheres to reach steady state representing an error of over 1000%! On the other hand, the modified diffusive flux model is constructed to reproduce the experimental result.

Although the modifications discussed in this research were only incorporated into the diffusive flux model, they could equally well be applied to the suspension balance model. In fact, the results of Fang et al. (2002), actually infer the same linear relationship between particle radius and diffusion coefficient as they determined a different diffusion coefficient for each bulk concentration considered.

Finally, this modifications to the diffusive flux model has only been tested for the wide-gap Couette apparatus. Experimental results for pipe and channel flow are quite different (Hampton et al., 1997, 1993) where it has been reported that the scaling of the migration rate with particle diameter is sub-quadratic! However, this contrasting result may be explained by the nonlocal part of the shear rate, $\dot{\gamma}_{NL}$. For these Poiseuille flows, as the local shear rate goes to zero near the centerline, the nonlocal shear rate becomes more and more dominant compared to the local shear rate in determining the nonlinearity parameter. In these regions, the $a$ in $\dot{\gamma}_{NL}$ cancels the $a$ in the numerator of the nonlinearity parameter, $\xi_{nl}$, restoring the $a^2$ scaling. That is, shear-rate averaging effects across the suspended particle may reduce the scaling rate of migration in regions where the shear rate approaches zero. This is the topic of current research by our group.

## Acknowledgements

This work was partially supported by the U.S. Department of Energy (DOE) Grant DE-FG02-05ER25705. This financial support does not constitute an endorsement by the DOE of the views expressed in this paper. Los Alamos National Laboratory, an affirmative action/equal opportunity employer, is operated by the Los Alamos National Security, LLC for the National Nuclear Security Administration of the U.S. Department of Energy under contract DE-AC52-06NA25396. Additional funding for this project was provided by the Los Alamos National Laboratory Directed Research and Development Program. Sandia is a multiprogram laboratory operated by Sandia Corporation, a Lockheed Martin Company for the United States Department of Energy's National Nuclear Security Administration under Contract DE-AC04-94AL85000. The authors would like to acknowledge the support of DOE ASCR's Multiscale Mathematics program. This material was based on work supported by the National Science Foundation, while Marc Ingber was working at the Foundation.

## References

Abbott, J.R., Tetlow, N., Graham, A.L., Altobelli, S.A., Fukushima, E., Mondy, L.A., Stephens, T.S., 1991. Experimental observation of particle migration in concentrated suspensions: Couette flow. J. Rheol. 35 (5), 773–795.

Buyevich, I.A., 1995. Particle distribution in suspension shear flow. Chem. Eng. Sci. 51 (4), 635–647.

Chow, A.W., Sinton, S.W., Iwamiya, J.H., 1994. Shear-induced particle migration in Couette and parallel-plate viscometers: NMR imaging and stress measurements. Phys. Fluids 6, 2561–2575.

Fang, Z., Mammoli, A.A., Brady, J.F., Ingber, M.S., Mondy, L.A., Graham, A.L., 2002. Flow-aligned tensor models for suspension flows. Int. J. Mult. Flow 28 (1), 137–166.

Gulmus, S.A., Yilmazer, U., 2005. Effect of volume fraction and particle size on wall slip in flow of polymeric suspensions. J. Appl. Polym. Sci. 98, 439–448.

Hampton, R.E., Mammoli, A.A., Graham, A.L., Altobelli, S.A., 1997. Migration of particles undergoing pressure-driven flow in a circular conduit. J. Rheol. 41 (3), 621–639.

Hsiao, S.-C., Christensen, D., Ingber, M.S., Mondy, L.A., Altobelli, S.A., 2003. Particle migration rates in a Couette apparatus. In: Mammoli, A.A., Brebbia, C.A. (Eds.), Computational Methods in Multiphase Flow II. Southampton, pp. 241–251.

Hsiao, S.-C., Christensen, D., Ingber, M.S., Mondy, L.A., Altobelli, S.A., 2005. Particle migration rates in a Couette apparatus. J. Mech. 21 (2), 71–75.

Ingber, M.S., Feng, S., Graham, A.L., Brenner, H., 2008. The analysis of self-diffusion and migration of rough spheres in nonlinear shear flow using a traction-corrected boundary element method. J. Fluid Mech. 598, 267–292.

Jana, S.C., Kapoor, B., Acrivos, A., 1995. Apparent wall slip velocity coefficients in concentrated suspensions of noncolloidal particles. J. Rheol. 39 (6), 1123–1132.

Jenkins, J.T., McTigue, D.F., 1990. Transport process in concentrated suspensions: the role of particle fluctuations. In: Joseph, D.D., Schaeffer, D.G. (Eds.), Two Phase Flows and Waves. Springer-Verlag, New York, pp. 70–79.

Kalyon, D.M., 2005. Apparent slip and viscoplasticity of concentrated suspensions. J. Rheol. 49 (3), 621–640.

Koh, C.J., Hookham, P., Leal, L.G., 1993. An experimental investigation of concentrated suspension flows in a rectangular channel. J. Fluid Mech. 266, 695–719.

Krieger, I.M., 1972. Rheology of monodisperse latices. Adv. Colloid Int. Sci. 3, 111–136.

Leighton, D., Acrivos, A., 1987. The shear-induced migration of particles in concentrated suspensions. J. Fluid Mech. 181, 415–439.

Miller, R.M., Morris, J.F., 2006. Normal stress-driven migration axial development pressure-driven flow of concentrated suspensions. J. Non-Newt. Fluid Mech. 135, 149–165.

Mondy, L.A., Grillet, A.M., Henfling, J., Ingber, M.S., Graham, A.L., Brenner, H., 2005. Apparent slip at the surface of a ball spinning in a concentrated suspension. J. Fluid Mech. 538, 377–397.

Morris, J.F., Boulay, F., 1999. Curvilinear flows of noncolloidal suspensions: the role of normal stresses. J. Rheol. 43, 1213.

Morris, J.F., Brady, J.F., 1998. Pressure-driven flow of a suspension: Buoyancy effect. Int. J. Mult. Flow 24 (1), 105–130.

Nott, P., Brady, J.F., 1994. Pressure-driven flow of suspensions: principles and computational methods. J. Fluid Mech. 275, 157–199.

Phillips, R.J., Armstrong, R.C., Brown, R.A., Graham, A.L., Abbott, J.R., 1992. A constitutive equation for concentrated suspension that accounts for shear-induced particle migration. Phys. Fluids A 4 (1), 30–40.

Pozarnik, M., Skerget, L., 2003. Boundary element method numerical model based on mixture theory of two-phase flow. In: Mammoli, A.A., Brebbia, C.A. (Eds.), Computational Methods in Multiphase Flow II. Southampton, pp. 3–12.

Shapley, N.C., Brown, R.A., Armstrong, R.C., 2004. Evaluation of particle migration models based on laser Doppler velocimetry measurements in concentrated suspensions. J. Rheol. 48 (2), 255–279.

Soltani, F., Yilmazer, U., 1998. Slip velocity and slip layer thickness in flow of concentrated suspensions. J. Appl. Polym. Sci. 70, 515–522.

Subia, S.R., Ingber, M.S., Mondy, L.A., Altobelli, S.A., Graham, A.L., 1998. Modelling of concentrated suspensions using a continuum constitutive equation. J. Fluid Mech. 373, 193–219.

Tetlow, N., 1997. Demixing of suspensions in a wide-gap Couette device. Master's thesis, University of New Mexico.

Tetlow, N., Graham, A.L., Ingber, M.S., Subia, S.R., Mondy, L.A., Altobelli, S.A., 1998. Particle migration in a Couette apparatus: experiment and modeling. J. Rheol. 42 (2), 307–327.